PHOTOCATALYTIC DECOLORIZATION STUDY OF METHYL ORANGE BY TiO_2-CHITOSAN NANOCOMPOSITES

Imelda Fajriati[1,*], Mudasir[2], and Endang Tri Wahyuni[2]

[1]*Department of Chemistry, State Islamic University Sunan Kalijaga, Jl. Marsda Adisucipto Yogyakarta 55281, Indonesia*

[2]*Department of Chemistry, Faculty of Mathematics and Natural Sciences, Universitas Gadjah Mada, Sekip Utara Yogyakarta 55281, Indonesia*

Received January 20, 2014; Accepted July 17, 2014

ABSTRACT

The photocatalytic decolorization of methyl orange (MO) by TiO_2-chitosan nanocomposite has been studied. This study was started by synthesizing TiO_2-chitosan nanocomposites using sol-gel method with various concentrations of Titanium(IV) isopropoxide (TTIP) as the TiO_2 precursor. The structure, surface morphology, thermal and optical property of TiO_2-chitosan nanocomposite were characterized by X-ray diffraction (XRD), fourier transform infra red (FTIR) spectroscopy, scanning electron microscopy (SEM), thermogravimetric analysis (TGA), and diffuse reflectance ultra violet (DRUV) spectroscopy. The photocatalytic activity of TiO_2-chitosan nanocomposite was evaluated by photocatalytic decolorization of methyl orange as a model pollutant. The results indicate that the particle size of TiO_2 increases with increasing of the concentration of TTIP, in which TiO_2 with smallest particle size exhibit the highest photocatalytic activity. The highest photocatalytic decolorization was obtained at 5 h of contact time, initial concentration of MO at 20 ppm and at solution pH of 4. Using these conditions, over 90% of MO was able to be decolorized using 0.02 g of TiO_2-chitosan nanocomposite under UV light irradiation. The TiO_2-chitosan nanocomposite could be reused, which meant that the TiO_2-chitosan nanocomposites can be developed as an effective and economical photocatalyst to decolorize or treat dye in wastewater.

Keywords: *TiO_2-chitosan nanocomposites; decolorization; methyl orange*

ABSTRAK

Telah dilakukan studi reaksi dekolorisasi metil orange (MO) terkatalisis nanokomposit TiO_2-kitosan. Studi diawali dengan sintesis nanokomposit TiO_2-kitosan menggunakan metode sol gel dengan variasi konsentrasi titanium (IV) isopropoksida (TTIP) sebagai prekursor. Struktur, morfologi, sifat termal dan optis dikarakterisasi menggunakan X-ray diffraksi (XRD), Fourier transform infra red (FTIR) spektroskopi, scanning electron microscopy (SEM), thermogravimetric analysis (TGA), dan diffuse reflectance ultra violet (DRUV) spektroskopi. Aktivitas fotokatalitik nanokomposit TiO_2-kitosan diuji dalam reaksi fotokatalisis dekolorisasi terhadap larutan metil orange (MO) sebagai model polutan. Hasil eksperimen menunjukkan bahwa kenaikan konsentrasi TTIP akan meningkatkan ukuran partikel TiO_2, di mana ukuran partikel TiO_2 terkecil menghasilkan aktivitas fotokatalitik tertinggi. Reaksi dekolorisasi fotokatalitik tertinggi dicapai menggunakan waktu kontak selama 5 jam, konsentrasi MO mula-mula sebesar 20 ppm dan pH 4. Pada kondisi tersebut, lebih dari 90% MO dapat terdekolorisasi menggunakan 0,02 g fotokatalis nanokomposit TiO_2-kitosan. Lebih lanjut, nanokomposit TiO_2-kitosan juga dapat diregenerasi, hal ini berarti nanokomposit TiO_2-kitosan dapat dikembangkan menjadi fotokatalis yang efektif dan ekonomis untuk mendekolorisasi zat warna dalam limbah cair.

Kata Kunci: *nanokomposit TiO_2-kitosan; dekolorisasi; metil orange*

INTRODUCTION

Methyl orange (MO) is one of the azo dyes that has been widely used in many applications because it is inexpensive and relatively stable during the dyeing. Methyl orange (MO) has a variety of uses such as in textiles, foodstuffs, pulp and paper, and leather industry. About 20% of synthetic dyes produced are lost in waste stream during dyeing process. The direct release of these complex dyes and their products to the environment may cause serious problems. The biodegradation of dyes in the aquatic ecosystem take a long time, and therefore can cause dramatic consequences such as esthetic pollution, and perturbations in aquatic life [1].

* Corresponding author. Tel/Fax : +62-274-4333257
Email address : imel257_75@yahoo.co.id

Many physical and chemical processes have been applied in dye removal, including coagulation and flocculation, biosorption, photo-decomposition and ultrafiltration, membrane and electrochemical processes [2]. However, such processes still possess a number of disadvantages, as they need waste disposal sites and more advanced treatment to reduce the waste toxicity. Furthermore, treatment of liquid waste with such methods may take a longer time, much more energy as well as price.

Photocatalytic treatment is an attractive alternative technique for the removal of dyes. It can result in complete mineralization of organic compounds to carbon dioxide, water and mineral acids. The major advantages of photocatalysis technology are as follows [3]: (i) Photocatalysis offers a good substitute for the energy-intensive conventional treatment methods for using renewable and pollution-free solar energy, (ii) This process can be used to destroy a variety of organic hazardous compounds in different wastewater streams, and (iii) Secondary waste generation is minimalized.

Among many photocatalysts that have been used, so far TiO_2 is one of photocatalyst that has been found to be good for treating dye containing waste. However, its application in photocatalytic degradation is limited due to difficulty in separating the photocatalyst and it is normally less active photocatalyst. In order to address the problem, a number of researchers have focuses their attention to prepare nano-size TiO_2 as well as modify TiO_2 by immobilization in a host material by making TiO_2 in the nanoparticle. TiO_2 nanoparticle can improve their photocatalytic activity because then surface area increases as a result of smaller particle size. It is concomitant with enhancement of chemical activity of TiO_2. The chemical activity is connected with several structural and electronic size-related effects and also the photochemical and photophysical activities by reduction of light scattering [4]. In addition, immobilization of TiO_2 in a host material may leads to easier handling and separating of TiO_2 from the water phase easier.

A number of host materials have been used as supporting agent for TiO_2 immobilization, such as resin [5], zeolite [6], active carbon [7], silica [8] and fiberglass [9]. The resulted materials are usually quite rigid, expensive and not environmentally friendly. The recent research demonstrated that biomaterials are considered as a good choice for supporting inorganic materials such as metal oxide photocatalyst, resulting in organic/inorganic hybrid and nanocomposites [10-11]. Chitosan has been reported to be one of biomaterials deemed suitable and excellent bio-matrix for the synthesis of nanosized particles or quantum dots of various inorganic photocatalysts. Chitosan can effectively prevent nanoparticles from agglomeration during growth [12]. Immobilization of TiO_2 nanoparticles in the chitosan matrix is expected to solve the recovery problem of nanosized powder materials.

In the present study, therefore we investigated the use of chitosan as an alternative supporting agent to prepare TiO_2 nanoparticle photocatalyst. The synthesis of TiO_2 nanoparticles was carried out *in-situ* in the chitosan matrix at room temperature followed by an aging process [13]. The photocatalytic activity of the obtained photocatalyst was systematically examined in the decolorization process of a model dye pollutant.

Methyl orange (MO) was selected as a model dye pollutant to evaluate the decolorization activity of the photocatalytic TiO_2-chitosan nanocomposites. The synthesis of TiO_2-chitosan nanocomposite was conducted using various concentrations of Titanium(IV) isopropoxide (TTIP) as the TiO_2 precursor in order to obtain the nanocomposite composition with the highest photocatalytic activity. A number of factors influencing the photocatalytic decolorization of the dye were studied, including the contact time between photocatalyst and MO, the initial pH as well as the initial concentration of MO solution. As a reference, TiO_2 powder (bulk) was also used in the photocatalytic process of MO decolorization using the same conditions.

EXPERIMENTAL SECTION

Materials

Titanium(IV) isopropoxide (TTIP) was purchased from Sigma-Aldrich. Acetic acid 99.8% and Methyl orange ($C_{14}H_{14}O_3N_3SNa$) was purchased from Merck. Chitosan (with 87% degrees of deacetylation) was purchased from Biotech Surindo Cirebon of Indonesia. aquabidestilate and deionized water were supplied by Pharmaceutical Laboratories Jakarta. All chemicals were of reagent grade, and no additional purification was done.

Instrumentation

Magnetic stirrer hotplate (Cimarec Barnstead Thermolyne) was used to prepare the solutions, centrifugation was carried out using Boeco C-28 Centrifuge (Model BOE 1205-13, Boeckel & Co, Hamburg, Germany) and the drying process was done using an oven (Thermoline Electric from Heareus). The photocatalytic decolorization of MO was conducted using a closed photoreactor equipped with 40 watt of UV lamp, operated at 290–390 nm as well as magnetic stirrer [14].

Thermogravimetric analysis (TGA) (16-thermogravimetric Perkin Elmer) was used to investigate the thermal stability of the sample. Each

sample was heated from 30 °C to 900 °C at the scanning rate of 10 °C. min^{-1} under dynamic nitrogen atmosphere. The structure, phase composition and the average crystallite size of TiO_2-chitosan nanocomposites were determined using the powder and plate XRD technique. The patterns were recorded on a Shimadzu X-ray Diffractometer 6000 (XRD) using Cu K*α* X-ray tube at 1.5460 Å, 40 kV and 30mA with scan steps of 1° min^{-1} over the 2*θ* range of 20°–80°. The chemical functional groups were examined using a Fourier Transform Infrared Spectrophotometer (Shimadzu) and a KBr pellets in the wavelength range of 400.0–4000.0 cm^{-1}. The surface morphology was studied by scanning electron microscope (SEM) using JEOL JSM–6360. The optical property was studied by Diffuse Reflectance UV-VIS Spectra Shimadzu UV 1700 Pharmaspec. The decolorization process of MO was monitored by Spectrophotometric Ultraviolet Visible Shimadzu at 464 nm.

Procedure

Preparation of TiO_2 sol by aging at room temperature

The chitosan solution was prepared by dissolving 3 g chitosan in 100 mL acetic acid 1% solution, followed by vigorous stirring at room temperature for 24 h. Fifty milliliters of Titanium(IV) isopropoxide (TTIP) was added dropwise into 500 mL of deionized water containing 50 mL of acetic acid solution under vigorous stirring at room temperature for 24 h. The obtained mixture is labeled as TTIP sol. Freshly prepared TTIP sol was then stored without stirring at room temperature and atmospheric pressure. It became transparent within one week.

Preparation of TiO_2-chitosan nanocomposites and TiO_2 powders

TTIP sol was used to prepare TiO_2-chitosan nanocomposites by sol-gel technique. Different amount of the TTIP sol was added to chitosan solution 3% (w/v) to reach the desired concentrations of TTIP (mol/L): 0.13, 0.33, 0.65 and 1.3, under vigorous stirring at room temperature for 24 h. The resulted nanocomposites was then stored without stirring at room temperature and atmospheric pressure in two weeks (14 days). The nanocomposites was then dried at 80 °C for 60 min in a preheated oven. Finally, the nanocomposites was washed with aquabidestilate until pH 6–7, and then dried again at 80 °C for 60 min in a preheated oven. Various TTIP concentration of 0.13, 0.33, 0.65 and 1.3 mol/L were used to prepare different TiO_2-chitosan nanocomposites to produce samples named as NK 0.13, NK 0.33, NK 0.65 and NK 1.3 respectively.

TiO_2 powder (bulk): Fifty milliliters of 3% sodium carbonate solution were added dropwise into the corresponding TTIP sols under vigorous stirring until precipitation occurred. The formed suspension were centrifuged at 3000 rpm for 5 min, followed by removal of the liquid phase. The precipitates of TiO_2 bulk were then washed with water and dried at 100 °C for 60 min in a preheated oven. Finally, the precipitates of TiO_2 bulk crushed to TiO_2 powder.

Photocatalytic decolorization of methyl orange (MO) by TiO_2-chitosan nanocomposites

0.02 g of each TiO_2-chitosan nanocomposite (NK 0.13, NK 0.33, NK 0.65 and NK 1.3) were added to 20 mL of MO (20 mg/L) in an Erlenmeyer flask and placed in the photoreactor, and it was allowed to react a different contact time (1–8 h, with one hour interval). Afterwards, the mixture was centrifuged at 3000 rpm for 5 min. The filtrate was taken out and measured by UV-Vis at 464 nm. This experiment was then repeated for different concentrations of MO (10, 20, 30, 40 and 50 mg/L) and pH (2, 3, 4, 5, 6, 7, 8). As a reference, TiO_2 powder (bulk) was also used for the photocatalytic process using the same conditions.

RESULT AND DISCUSSION

Characteristics of TiO_2-Chitosan Nanocomposites

FTIR Spectroscopy

Functional group of TiO_2-chitosan nano composites at various TTIP concentrations were characterized by Fourier Transform Infra Red (FTIR) spectroscopy. Fig. 1 compares the FTIR spectra of chitosan bulk, TiO_2 bulk and TiO_2-chitosan nanocomposites (NK 0.13, NK 0.33, NK 0.65 and NK 1.3).

Close examination of the absorption bands of the IR spectra of TiO_2, chitosan bulk and the IR spectra of the TiO_2-chitosan nanocomposite, it reveals that the IR spectra in general exhibit similar shifts of some the typical absorption bands as well as new absorption bands as TTIP concentration in the nanocomposites is varied. The IR spectra of TiO_2 and chitosan bulk clearly show a new wide O–Ti–O band at the range of 600–900 cm^{-1}, which can be ascribed to the presence of TiO_2 network on chitosan matrix. This interpretation is supported by the existence of inter-phase compatibility which can be observed from the appearance of bands at 962 cm^{-1} and 945 cm^{-1}, indicating that the interaction of Ti Lewis sites with the NH_2 groups from chitosan chain exists [15]. The increase in the band intensity probably corresponds to the increase of TTIP concentration in the nanocomposites.

In addition, the band shift at around 1427 cm^{-1} to 1404 cm^{-1} in TiO_2-chitosan nanocomposite can be attributed to the existence of protonated amino groups

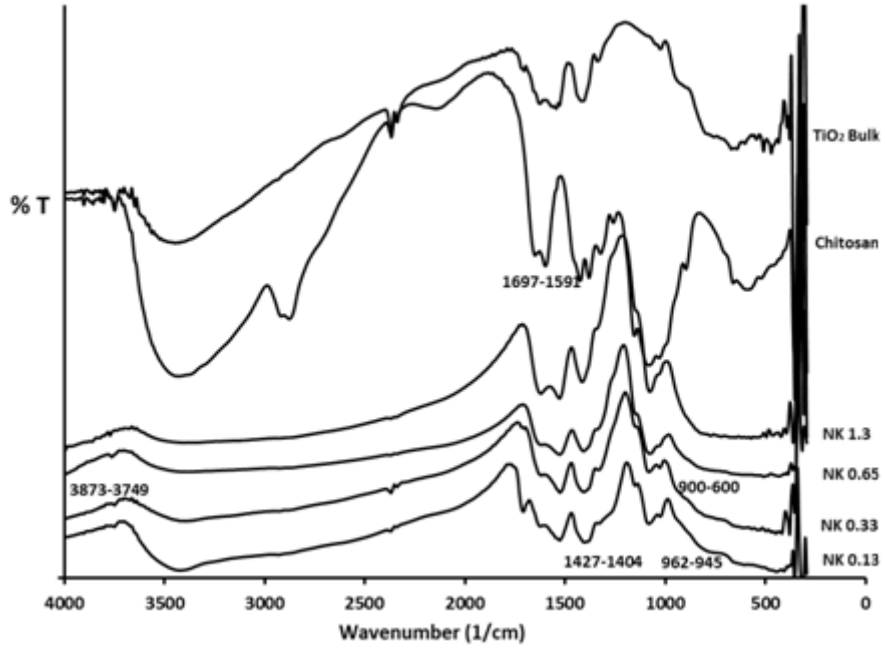

Fig 1. FTIR spectra of chitosan bulk, TiO_2 bulk and TiO_2–chitosan nanocomposites (NK 0.13, NK 0.33, NK.1.65 and NK 1.3)

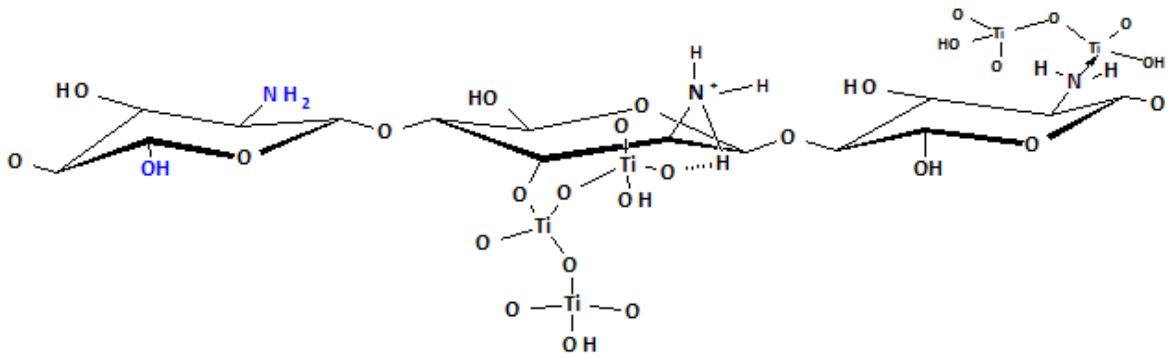

Fig 2. The hypothetic interaction between TiO_2 and chitosan

in the chitosan structure which forms hydrogen bond to Ti site [16]. In the region wavenumber of 3749 to 3873 cm^{-1}, the spectral transmittance also appears as sharper bands in TiO_2-chitosan nanocomposites, indicating that hydroxyl groups of chitosan has been attached to titania network. From this evidence, it can be assumed that hydrogen bond is one of the possible interactions between chitosan and TiO_2 [17]. The hypothetic interaction between chitosan and TiO_2 is illustrated in Fig. 2.

Some researchers has suggested that the formation of Lewis acid-base interaction and hydrogen bond between the functional groups in chitosan and other substances can also be considered as a way for chitosan to stabilize its interactions. Thus, the insertion of TiO_2 into the chitosan matrix may result in two possible interactions, hydrogen bond and Lewis acid-base interaction between the functional group of chitosan and Ti site as can be seen in Fig. 2.

Thermogravimetric Analysis (TGA)

The thermal stability of chitosan bulk and TiO_2-chitosan nanocomposites (NK 0.13, NK 0.33, NK 1.65 and NK 1.3), has been thoroughly investigated to determine the amount of TiO_2 particles bound to the chitosan matrix. The result of TGA measurement is shown in Fig. 3 as a TG curve.

As clearly seen in Fig. 3, TG curves of the TiO_2-chitosan nanocomposites at various TTIP concentrations for NK 0.13, NK 0.33, NK 0.65, and NK 1.3, exhibiting three distinct weight-loss stages. *The first stage* shows a weight loss of about 20% started from 30 °C up to 300 °C. This weight loss is attributed to the release of surface-bound water or physically

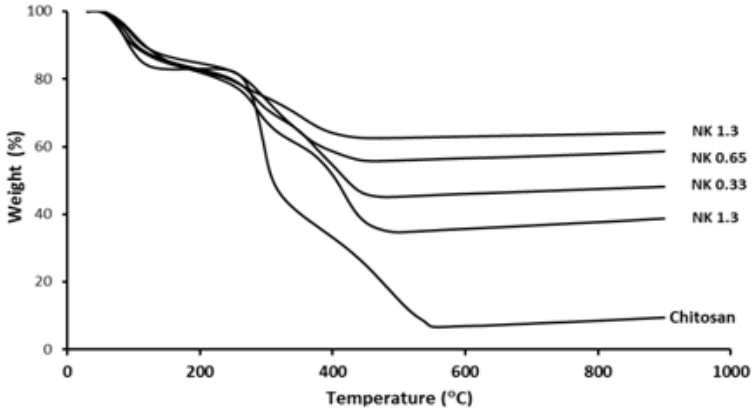

Fig 3. TG curve of chitosan bulk and TiO_2–chitosan nanocomposites (NK 0.13, NK 0.33, NK 0.65, and NK 1.3)

Table 1. Influence of TTIP concentrations (mol/L) introduced into the chitosan matrix on the amount of loaded TiO_2

Types of TiO_2 – chitosan nanocomposite	[TTIP] (mol/L)	Amount of loaded TiO_2 in the TiO_2–chitosan nanocomposite (% w/w, TGA)
NK 0.13	0.13	30
NK 0.33	0.33	35
NK 0.65	0.65	45
NK 1.3	1.30	55

absorbed water on the surface of chitosan bulk and TiO_2-chitosan nanocomposites. *The second stage* weight loss started from 250 to 450 °C observed for TiO_2-chitosan nanocomposite may be correlated to the decomposition of chitosan and vaporization and elimination of volatile products [18]. The weight loss at this stage can also be correlated with the amount of titania introduced/immobilized into the chitosan matrix frame. The increasing amount of the TTIP in the chitosan matrix results in the decrease of the decomposition temperature of nanocomposite due to less amount of chitosan available in the nanocomposites. *The third stage* of TG curve shows that the curves for TiO_2-chitosan nanocomposite reach a plateau at about 450 °C, indicating the complete degradation of chitosan. While chitosan bulk leaves weight percentage of residue of 10% at 900 °C which is proportional to the residual organic group [19], TiO_2-chitosan nanocomposite at the same temperature still have left weight of around or higher than 40% relative to their initial weight, suggesting that the TiO_2-chitosan nanocomposites exhibits better thermal stability than the chitosan bulk [16].

The influence of TTIP concentration introduced into the chitosan matrix on the weight of TiO_2 formed after complete thermal degradation for TiO_2-chitosan nanocomposites (%wt/wt) is summarized in Table 1.

Table 1 shows that the increase in TTIP concentration leads to the increase of the weight of TiO_2 formed in the TiO_2-chitosan nanocomposite. This indicates that the increase of TTIP concentration as TiO_2 precursor enhances the seed required for growth of TiO_2 crystal. As a result, the amount of TiO_2 that can be loaded into the TiO_2-chitosan nanocomposite also increases.

XRD Spectroscopy

X-Ray Diffraction (XRD) analysis was carried out to confirm the presence of TiO_2 polymorphs and crystal phases. X-Ray diffraction pattern of the TiO_2-chitosan nanocomposite at various TTIP concentrations is shown in Fig. 4. It can be seen that the only observed peaks are at 2θ of 25.4°, 38.0° and 48.0° which characteristically correspond to anatase crystal phase, and there is no single peak observed for brookite in the nanocomposite, suggesting that only TiO_2 anatase is formed during the preparation of nanocomposites.

Striking examination of Fig. 4 also reveals that the increase in the TTIP concentration increases the amount of the crystal phase in the TiO_2-chitosan nanocomposite, as indicated by higher relative intensities of the peaks for NK 1.3. This result is in good agreement with that of previous finding from TGA analysis. The peak sharpness of the XRD patterns also indicates the particle size of TiO_2, the sharper the band, the smaller the particle size. The crystallite size of TiO_2 in nanocomposite can be calculated from XRD line broadening using the Scherrer equation:

$$L = \frac{K\lambda}{\beta \cos\theta} \quad (1)$$

where L is the crystallite size of TiO_2 in nanocomposites, K is a constant (0.94), λ is the wavelength of X-ray (CuKα = 1.54056 ° A), ß is the true

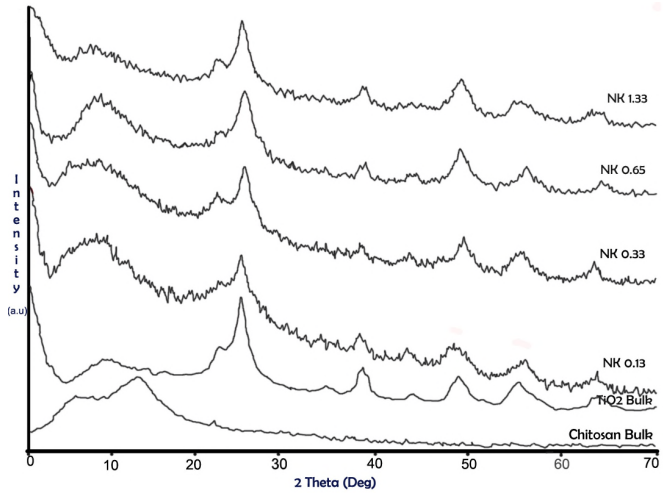

Fig 4. XRD Patterns of chitosan bulk, TiO_2 bulk, and TiO_2–chitosan nanocomposite (NK 0.13, NK 0.33, NK 0.65, and NK 1.3)

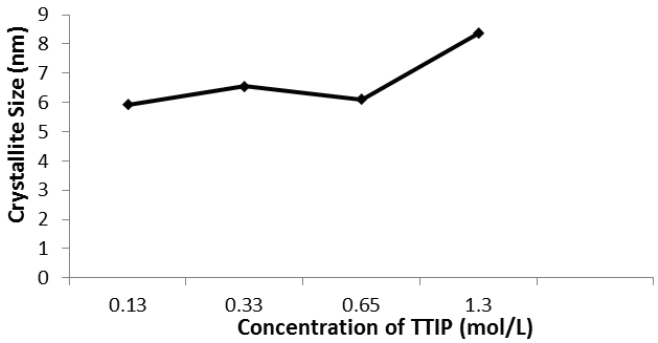

Fig 5. Crystallite size of anatase in TiO_2–chitosan nanocomposite (NK 0.13, NK 0.33, NK 0.65, and NK 1.3)

half-peak width, and θ is the half diffraction angle of the centroid of the peak in degree. The average crystallite sizes of anatase in TiO_2-chitosan nanocomposite in Fig. 5.

Fig. 5 gives the typical values of anatase crystallite size in TiO_2-chitosan nanocomposite as calculated using Scherrer`s equation. It is clearly shown that the crystallite size of anatase is in the range of 5–10 nm. This size of TiO_2 in chitosan indicates that chitosan biopolymer is able to hinder the crystal growth of titania as indicated by the uniformed value of the particle size of TiO_2. Fig. 5 also shows that increasing TTIP concentration (NK 0.13 up to NK 1.3) results in the increase of the particle size of TiO_2. Thus, it is obvious that at higher TTIP concentration, the TiO_2 nanoparticle seeds formed during the preparation became relatively close to each other and this shorter inter-particle distance give good facilities for the particle growth. Therefore, it may then be concluded that in addition to the chitosan matrix that gives limited space for TiO_2 to grow, the precursor concentration can also contribute to the formation of the particle size [20].

It was also observed, however, that there is a trend change when TTIP concentration is increased for NK 0.13 to NK 0.33, where the crystallite size of TiO_2 is becoming smaller with the increase in the concentration of TTIP. This is probably due to the structural change of chitosan from a stretched chain into a coiled one, and finally it changes into inter-twisted coils or four-fold helix to produce an asymmetric disaccharide unit [21]. This process is expected to be the limiting factor of the crystal growth. Further increase of TTIP concentrations at higher concentration than 0.65 mol/L as found in NK 0.65, however, causes TTIP to form bulkier structure outside the structure of chitosan, leading to the formation of larger particles.

According to Wang et al. [20], chitosan plays an important role in TiO_2 nanoparticles growth. The proportion of chitosan between acetylated and non-acetylated residues is considered to be responsible for the balance between hydrophilic and hydrophobic interactions. Researchers have concluded that chitosan molecular chains are able to form some hydrophobic microdomains because of their self aggregation behavior. Chitosan chains may undergo structural transformation from stretched chains into coils and further transformed into inter-twisted coils which is a hydrophobic microdomains with increasing concentration of TTIP during the aggregation process. The macromolecule structure of inter-twisted coils becomes quite compact so that the movement of the macromolecule is restricted. Such properties of chitosan enable the formation of a dispersed chitosan nanoparticles. As a result, TiO_2 nucleation and growth are well controlled.

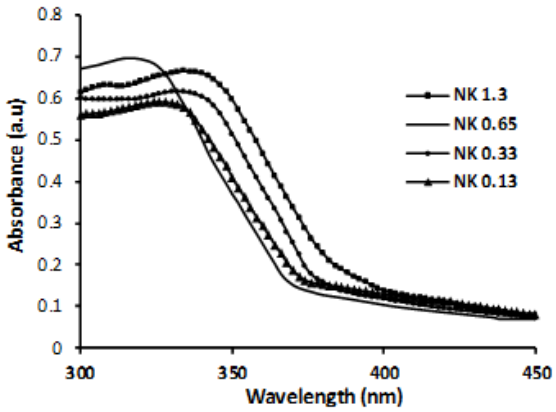

Fig 6. Ultraviolet spectra of nanocomposite TiO_2-chitosan (NK 0.13, NK 0.33, NK 0.65 and NK 1.3)

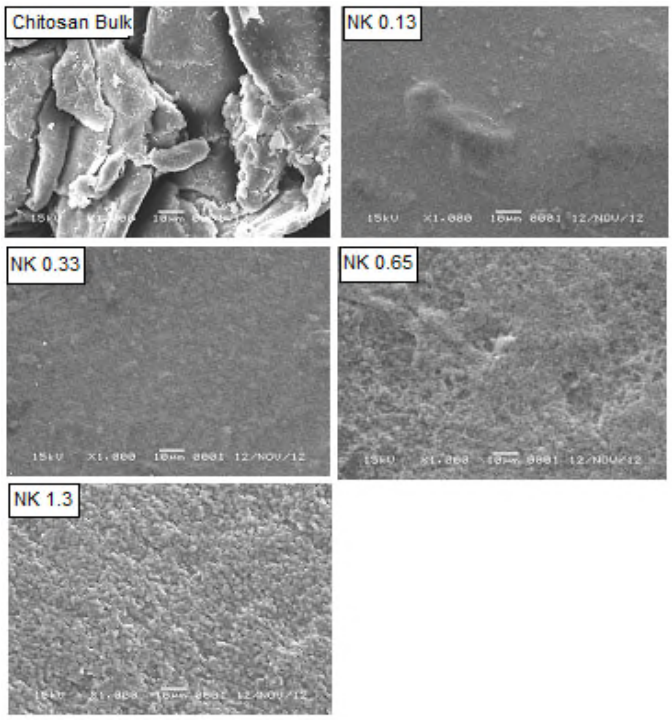

Fig 7. SEM images of chitosan bulk and TiO_2-chitosan nanocomposite (NK 0.13, NK 0.33, NK 0.65 and NK 1.3)

Table 2. The band gap energy of TiO_2-chitosan nanocomposites

Type of TiO_2-Chitosan Nanocomposite	Wavelength Edge (nm)	Eg (eV)
NK 0.13	388	3.192
NK 0.33	391	3.166
NK 0.65	380	3.258
NK 1.3	403	3.073

DR-UV Spectroscopy

Diffuse Reflectance Ultraviolet (DR-UV) Spectroscopy has been used to investigate optical properties and electronic band of TiO_2-chitosan nanocomposite at various TTIP concentrations. Fig. 6 shows the absorption spectra of the TiO_2-chitosan nanocomposites (NK 0.13, NK 0.33, NK 0.65, and NK 1.3). From this figure, it is observed that the TiO_2-chitosan nanocomposite exhibits an absorption edge ranging from 300 to 450 nm which corresponds to the absorption edge of semiconductor material.

It is clear that the increase in TTIP concentration shifts the absorption bands of TiO_2 to a higher wavelength (red shift), which also indicates an increase in particle size of TiO_2. This should mean that the particle size can be arranged as NK 0.13 < NK 0.33 < NK 1.3. However, the NK 0.65 has the shortest λ_{max}, indicating that its particle size is the smallest. This result agrees very well with that obtained from the calculation of particle size using Scherrer equation as previously discussed.

Table 2 shows the band gap energy of TiO_2-chitosan nanocomposites obtained from DR-UVS analysis. The band gap (Eg) determination has been extracted by calculating the absorbance of TiO_2-chitosan nanocomposites, while the edge wavelength is obtained by extrapolating the wavelength curve (Fig. 6) to intersect with X-axis [22].

As can be seen in Table 2, the increase in TTIP concentration in the chitosan matrix for NK 0.13 up to NK 1.3 increases the amount and bulk of TiO_2 formed in TiO_2-chitosan nanocomposite. The bulk of TiO_2 results in the increase of the particle size and therefore decreases the band gap energy. The result of the calculation of band gap energy is in agreement with the result obtained from the determination of TiO_2 particle size as previously discussed in Fig. 6, i.e. the increase in particle size gives rise to the lower band-gap energy.

SEM images

In this study Scanning Electron Microscope (SEM) has been used to analyze the morphology of the TiO_2-chitosan nanocomposite. The morphology of the TiO_2-chitosan nanocomposites for NK 0.13, NK 0.33, NK 0.65 and NK 1.3 can be observed from SEM images in Fig. 7.

Fig. 7 shows the change in the morphology and texture of the surface of TiO_2-chitosan nanocomposite. The images show that there is an increasing roughness throughout the surface of the TiO_2-chitosan nanocomposite with the increase of loaded titania. It can also be seen that the macroreticular structure of TiO_2 particles observed on the surface area of TiO_2-chitosan nanocomposite increases tremendously and concurrently as TTIP concentration in the matrix is elevated. The homogeneous dispersion and the blurred surface on the images indicate the existence of interaction of the polymer layers on the particle surface. The uniform or homogeneous dispersion of spherical

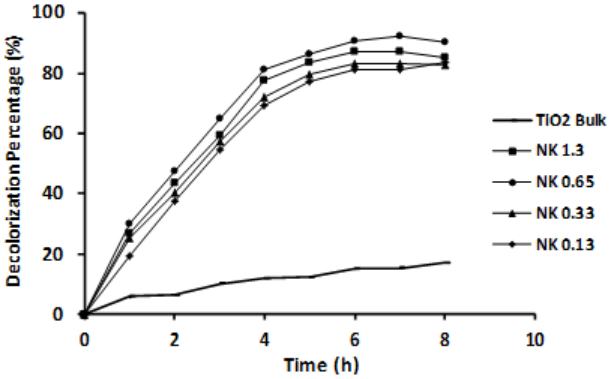

Fig 8. The influence of contact time on the photocatalytic decolorization of methyl orange (MO) by TiO_2 bulk and TiO_2-chitosan nanocomposites for NK 0.13, NK 0.33, NK 0.65 and NK 1.3 (MO concentration: 20 ppm; TiO_2 bulk and TiO_2-chitosan nanocomposite dosage: 0.02 g)

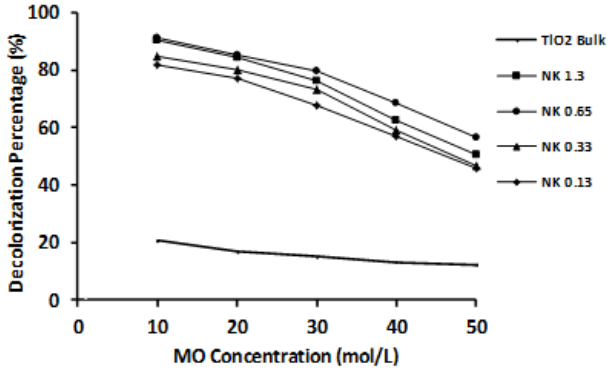

Fig 10. Influence of initial concentration of MO solution on the photocatalytic decolorization of methyl orange (MO) by TiO_2 bulk and TiO_2-chitosan for NK 0.13, NK 0.33, NK 0.65 and NK 1.3 (MO concentration: 20 ppm; TiO_2 bulk and TiO_2-chitosan nanocomposite dosage: 0.02 g)

particles is the outcome of synthesis process that takes place during the condensation stage. Homogeneous dispersion of TiO_2 nanoparticle in chitosan matrix is one of the most important factors to increase the photocatalytic activity of the nanocomposites [23].

Photocatalytic Decolorization of Methyl Orange by TiO_2-Chitosan Nanocomposites

Influence of contact time, pH and initial concentration of MO solution

Contact time, pH and initial concentration of MO solution are important parameters to be studied systematically in this experiment. In real application, these parameters play an important role in dye wastewater treatment and become important parameters influencing photo-oxidation process. The influence of these parameters on the photocatalytic decolorization of

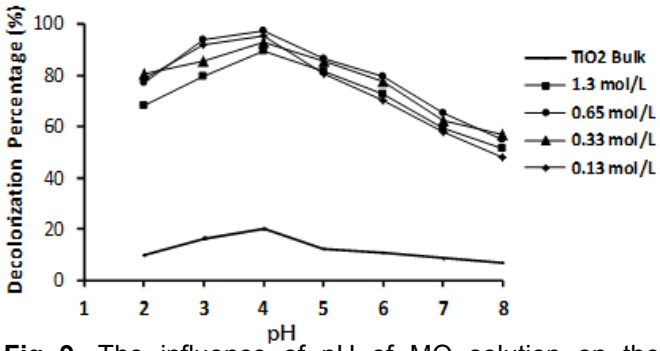

Fig 9. The influence of pH of MO solution on the photocatalytic decolorization of methyl orange (MO) by TiO_2 bulk and TiO_2-chitosan nanocomposites for NK 0.13, NK 0.33, NK 0.65 and NK 1.3 (MO concentration: 20 ppm; TiO_2 bulk and TiO_2-chitosan nanocomposite dosage: 0.02 g)

MO by TiO_2-chitosan nanocomposites was investigated using spectrometric analysis. The influence of contact time, pH and initial concentration on the photocatalytic decolorization of methyl orange is illustrated in Fig. 8-10.

Fig. 8-10 shows that the decolorization of MO using TiO_2 bulk is much lower than that of TiO_2-chitosan nanocomposites. This may be due to the particle size of TiO_2 bulk which is relatively larger, and thus reducing the effectiveness of the decolorization. At smaller particle size, quantum size effect occurs, resulting in a higher energy (favorable for the occurrence of photodegradation), which produces a much higher surface area of the titania. The higher surface area facilitates more contact between the photocatalyst and MO substrate. From the study it has been found that the optimum photocatalytic decolorization was achieved at 5 h of contact time. After 5 h, the photocatalytic decolorization did not show any significant increase as shown in Fig. 8.

The influence of pH of medium solution on the photocatalytic decolorization of MO can be seen in Fig. 9. The results show that the optimum photocatalytic decolorization of MO using TiO_2-chitosan nanocomposites is achieved at pH 3. The influence of pH on the decolorization process of MO might be related to the ionization state of MO as well as to the surface state of the photocatalyst, as well explained by Eq. 2 and 3, as also by Fig. 11.

The surface of TiO_2 can be denoted as >TiOH (titanol group) in aqueous solution. When pH of the solution is higher than 7, however, the surface state of photocatalyst becomes negatively charged according to the following ionization equilibrium [24]:

$$TiOH + OH^- \rightleftarrows TiO^- + H_2O \quad (2)$$

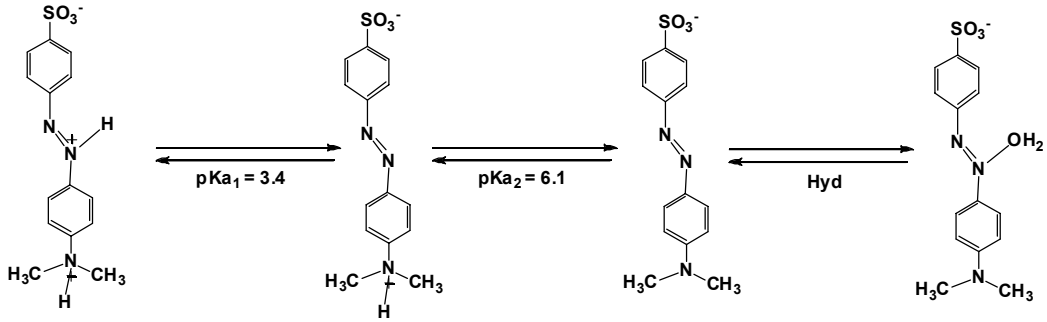

Fig 11. The effects of pH on the ionization state of methyl orange molecule

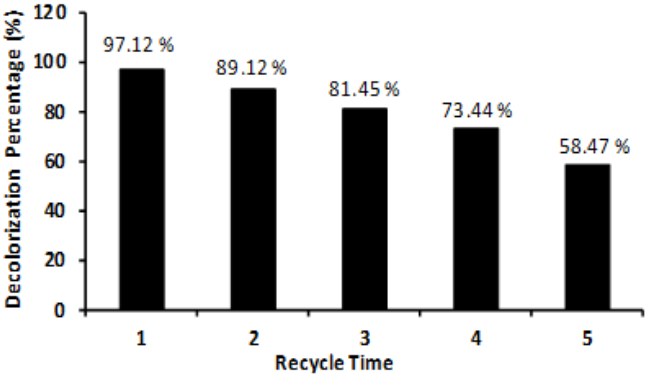

Fig 12. Recycle and reuse of NK 0.65 for MO decolorization (MO concentration: 20 mg/L; TiO_2-chitosan nanocomposite dosage: 0.02 g, pH 4; irradiation time: 5 h)

And at pH below 4, the ionization equilibrium is:

$$TiO + H^+ \rightleftarrows TiOH_2^+ \quad (3)$$

It can be seen from Eq. 2 and Eq. 3 that TiO^- species on the surface of photocatalyst is dominant at alkaline condition while $TiOH_2^+$ species is dominant at acidic condition. Similarly, the ionization state of MO is also pH dependent as illustrated in Fig. 11 [25].

According to Barka et al. [25], the rate constant of MO degradation decreases at pH higher than 3, which corresponds to the decreasing amount of $TiOH_2^+$ species. On the other hand, the adsorption of MO on the surface of photocatalyst becomes unfavorable at alkaline solution (higher pH) due to electrostatic repulsion forces between φ-SO_3^- of MO and TiO^- species on the surface of photocatalyst which are predominant in this range of pH. Therefore, it is reasonable to observe that the highest activity of photocatalytic decolorization of MO is achieved at pH 3.0 because at this pH the electrostatic attraction between the positively charged catalyst surface and MO anion is most favorable, leading to the increase the degree of adsorption of substrate in the surface of photocatalyst and hence speed up the photodecolorization process of MO.

The influence of the initial concentration of MO on the photocatalytic decolorization by TiO_2-chitosan nanocomposites were evaluated using different initial MO concentration of 10.0, 20.0, 30.0, 40.0 and 50.0 mg/L and the result is given in Fig. 11. In general, it can be observed that the decolorization percentage for all variation of TTIP concentration decreases markedly with the increase in the initial dye concentration. As the amount of photocatalyst in the solution is constant, this decrease can be attributed to the capacity of TiO_2-chitosan nanocomposite in adsorbing ionic groups of dye compounds on the photocatalyst surface as the concentration of MO increases, thus the capability of photocatalyst to initiates photo-oxidation also decreases.

Recycling/Reuse of the TiO_2-chitosan nano composite

For the purpose of further practical implementation such as in the real waste water treatment, it is important to evaluate the stability and durability of photocatalyst. In this study, we have made the 5 running experiments using the same photocatalyst to test its stability and durability and the results are shown in Fig. 12. For each running experiment, the same photocatalysts have been used for the decolorization of freshly prepared MO solutions under similar conditions after filtering, washing and drying photocatalyst that has been used in the previous running experiment.

As can be seen in Fig. 12, the percentage of MO decolorization slightly decreases after the second running/cycle. The results indicate that the photocatalytic activity of the TiO_2-chitosan nanocomposite also gradually decreases at third application and continue to decrease up to around 58.47% at fifth application/running. The decrease of decolorization percentage may be due to the coverage of active site of the surface of photocatalyst by intermediate products or MO molecules left in the nanocomposite materials, which could not be desorbed completely during the washing of photocatalyst. However, 58.47% of MO was decolorized successfully for the 5th use of the photocatalysts, which indicated

that the TiO_2-chitosan nanocomposite photocatalyst could be reused.

CONCLUSION

TiO_2-chitosan nanocomposite has been synthesized successfully by sol gel method using various TTIP concentrations. The characterization results suggest that TiO_2 nanoparticle has been formed in the chitosan matrix. The particle size of TiO_2 formed in the chitosan matrix is influenced by concentration of TTIP. Increasing TTIP concentration has been found to increase the particle size of TiO_2, leading to the lower band gap energy.

Results of photocatalytic decolorization study of MO demonstrate that smaller particle size of TiO_2 exhibits the higher photocatalytic activity. Experimental parameters including contact time, pH and initial concentration of MO solution affects significantly the photocatalytic activity. The optimum photocatalytic decolorization achieves at 5 h of contact time, MO initial concentration of 20 ppm and solution pH of 4. At these conditions of experiment, over 90% of MO has been able to decolorize using 0.02 g of TiO_2-chitosan nanocomposite under irradiation by UV light. From the recycling study of the TiO_2-chitosan nanocomposite, it has been observed that the photocatalyst is still able to decolorize MO solution up to five times of usage. This finding should indicate that TiO_2-chitosan nanocomposite photocatalyst could be used at a relatively low cost and therefore would be very beneficial in the practical application such as in the dye wastewater treatment.

ACKNOWLEDGEMENT

First author (IF) gratefully acknowledges The Institute for Educational Fund Management (LPDP), Ministry of Finance RI for the partial support of this research in the year of 2013.

REFERENCES

1. Guettai, N., and Amar, H.A., 2005, *Desalination*, 185 (1-3), 439–448.
2. Robinson, T., McMullan, G., Marchant, R., and Nigam, P., 2001, *Bioresour. Technol*., 77 (3), 247–255.
3. Kabra, K., Chaudhary, R., and Sawhney, R.L., 2004, *Ind. Eng. Chem. Res*., 43 (24), 7683–7696.
4. Fernández-García, M., Wang, X., Belver, C., Hanson, J.C., and Rodriguez, J.A., 2007, *J. Phys. Chem. C*, 111 (2), 674-682.
5. Wahyuni, E.T, Kunarti, E.S., and Mudasir, 2010, *J. Ion Exch.*, 21 (3), 304–309.
6. Fatimah, I., and Wijaya, K., 2006, *Teknoin*, 10 (4), 257–267.
7. Andayani, W., and Sumartono, A., 2007, *Indo. J. Chem.*, 7 (3), 238–241.
8. Pandiangan, D.K., and Simanjuntak, W., 2013, *Indo. J. Chem.*, 13 (1), 47–52.
9. Shifu, C., Xueli, C., Yaowu, T., and Mengyue, Z., 1998, *J. Chem. Technol. Biotechnol.*, 73 (3), 264–268.
10. Zhao, X., Li, Q., Zhang, X., Su, H., Lan, K., and Chen, A., 2010, *Environ. Prog. Sustainable Energy,* 30 (4), 567–575.
11. Zhaoa, X., Lv, L., Pan, B., Zhang, W., Zhang, S., and Zhang, Q., 2011, *Chem. Eng. J*., 170 (2-3), 381–394.
12. Chang, S., Kang, B., Dai, Y., Zhang, H., and Chen, D., 2011, *Nanoscale Res. Lett.*, 6 (1), 591.
13. Fajriati, I., Mudasir, and Wahyuni, E.T., 2013, *Proceeding of The 3rd Annual Basic Science Int`l Conference 2013*, Faculty Mathematic and Natural Science, University of Brawijaya, Malang of Indonesia, C1–C10.
14. Wahyuni, E.T., Aprilita, N.H., Hayu, A.H. F., Nurhayati, F.S., 2008, *Jurnal Manusia dan Lingkungan*, 15 (1), 10–15.
15. Al-Sagheer, F.A., and Merchant, S., 2011, *Carbohydr. Polym.*, 85 (2), 356–362.
16. Tao, Y., Pan, J., Yan, S., Tang, B., and Zhu, L., 2007, *Mater. Sci. Eng., B*, 138 (1), 84–89.
17. Li, Q., Su, H., and Tan, T., 2008, *Biochem. Eng. J*., 38 (2), 212–218.
18. Zhu, H., Jiang, R., Fu, Y., Guan, Y., Yao, J., Xiao, L., and Zeng, G., 2012, *Desalination*, 286, 41–48.
19. Zhua, H., Jiang, R., Xiao, L., Chang, Y., Guan, Y., Li, X., and Zeng, G., 2009, *J. Hazard. Mater.*, 169 (1-3), 933–940.
20. Wang, S., Huang, Y., Zheng, M., Wei, Y., Huang, S., and Gu, Y., 2011, *Adv. Polym. Technol.*, 30 (4), 269–275.
21. Lertworasirikul, A., Noguchi, K., Ogawa, K., and Okuyama, K., 2004, *Carbohydr. Res.*, 339 (4), 835–843.
22. Murphy, A.B., 2007, *Sol. Energy Mater. Sol. Cells*, 91 (14), 1326–1337.
23. Díaz-Visurraga, J., Meléndrez, M.F., García, A., Paulraj, M., and Cárdenas, G., 2010, *J. Appl. Polym. Sci.*, 116 (6), 3503–3515.
24. Hoffmann, M.R., Martin, S.T., Wonyong, C., and Bahnemann, D.W., 1995, *Chem. Rev*., 95 (1), 69–96.
25. Barka, N., Assabbane, A., Nounah, A., Dussaud, J., and Ichou, Y.A., 2008, *Phys. Chem. News,* 41, 85–88.